

Critical behavior and magnetocaloric effect in $\text{Mn}_3\text{Si}_2\text{Te}_6$

Yu Liu (刘育) and C. Petrovic

Condensed Matter Physics and Materials Science Department, Brookhaven National Laboratory, Upton, New York 11973, USA



(Received 11 April 2018; revised manuscript received 13 August 2018; published 27 August 2018; corrected 29 November 2018 and 14 January 2020)

The critical properties and magnetocaloric effect of semiconducting ferrimagnet $\text{Mn}_3\text{Si}_2\text{Te}_6$ single crystals have been investigated by bulk magnetization and heat capacity around T_c . Critical exponents $\beta = 0.41 \pm 0.01$ with a critical temperature $T_c = 74.18 \pm 0.08$ K and $\gamma = 1.21 \pm 0.02$ with $T_c = 74.35 \pm 0.05$ K are deduced by the Kouvel-Fisher plot, whereas $\delta = 4.29 \pm 0.05$ (3.40 ± 0.02) is obtained by a critical isotherm analysis at $T = 74$ (75) K. The magnetic exchange distance is found to decay as $J(r) \approx r^{-4.79}$, which lies between the mean-field and 3D Heisenberg models. Moreover, the magnetic entropy change $-\Delta S_M$ features a maximum at T_c , i.e., $-\Delta S_M^{\text{max}} \sim 2.53$ (1.67) $\text{J kg}^{-1} \text{K}^{-1}$ with in-plane (out-of-plane) field change of 5 T, confirming large magnetic anisotropy. The heat capacity measurement further gives $-\Delta S_M^{\text{max}} \sim 2.94 \text{ J kg}^{-1} \text{K}^{-1}$ and the corresponding adiabatic temperature change $\Delta T_{ad} \sim 1.14$ K with out-of-plane field change of 9 T.

DOI: [10.1103/PhysRevB.98.064423](https://doi.org/10.1103/PhysRevB.98.064423)

I. INTRODUCTION

Layered intrinsically ferromagnetic (FM) semiconductors hold great promise for both fundamental physics and applications in spintronic devices [1–5]. CrI_3 has recently attracted much attention since the long-range magnetism persists in monolayer with T_c of 45 K [3]. Intriguingly, the magnetism in CrI_3 is layer dependent, from FM in monolayer, to antiferromagnetic (AFM) in bilayer, and back to FM in trilayer [3]. It can further be controlled by electrostatic doping, providing great opportunities for designing magneto-optoelectronic devices [6,7].

Ternary $\text{Cr}_2\text{X}_2\text{Te}_6$ ($X = \text{Si}, \text{Ge}$) exhibit FM order below T_c of 32 K for $\text{Cr}_2\text{Si}_2\text{Te}_6$ and 61 K for $\text{Cr}_2\text{Ge}_2\text{Te}_6$, respectively [8–12], and also promising candidates for long-range magnetism in nanosheets [4,13,14]. Many efforts have been devoted to shed light on the nature of FM in this system [15–21]. Multiple domain structure types, self-fitting disks, and fine ladder structure within the Y-connected walls were observed by magnetic force microscopy [22], confirming two-dimensional (2D) long-range magnetism with non-negligible interlayer coupling [21]. $\text{Mn}_3\text{Si}_2\text{Te}_6$ is a little-studied three-dimensional (3D) analog of $\text{Cr}_2\text{Si}_2\text{Te}_6$ [23–25]. The $\text{Mn}_2\text{Si}_2\text{Te}_6$ layer is composed of MnTe_6 octahedra that are edge sharing within the ab plane (Mn1 site) and along with Si-Si dimers [Fig. 1(a)], similar to $\text{Cr}_2\text{Si}_2\text{Te}_6$. However, the layers are connected by filling one third of Mn atoms at the Mn2 site within interlayer, yielding a composition of $\text{Mn}_3\text{Si}_2\text{Te}_6$ [25]. Recent neutron diffraction experiment gives that $\text{Mn}_3\text{Si}_2\text{Te}_6$ is a ferrimagnet below $T_c \approx 78$ K and the moments lie within the ab plane [25].

In the present work we investigated the critical behavior of $\text{Mn}_3\text{Si}_2\text{Te}_6$ single crystal by using modified Arrott plot, Kouvel-Fisher plot, and critical isotherm analysis, as well as its magnetocaloric effect. Critical exponents $\beta = 0.41$ (1) with $T_c = 74.18$ (8) K, $\gamma = 1.21$ (2) with $T_c = 74.35$ (5) K, and $\delta = 4.29$ (5) at $T = 74$ K. The magnetic exchange distance is found to decay as $J(r) \approx r^{-4.79}$, which lies between mean-field and

3D Heisenberg models. The rescaled $-\Delta S_M(T, H)$ curves can well collapse onto a universal curve, confirming its nature of second order.

II. METHODS

A. Experimental details

Single crystals of $\text{Mn}_3\text{Si}_2\text{Te}_6$ were fabricated by melting stoichiometric mixture of Mn (3N, Alfa Aesar) chip, Si (5N, Alfa Aesar) lump and Te (5N, Alfa Aesar) shot. Starting materials were vacuum sealed in a quartz tube, heated to 1100 °C over 20 h and then cooled to 850 °C at a rate of 1 °C/h. X-ray diffraction (XRD) data were taken with Cu K_α ($\lambda = 0.15418$ nm) radiation of a Rigaku Miniflex powder diffractometer. The magnetization and heat capacity were collected in Quantum Design MPMS-XL5 and PPMS-9 systems. The magnetic entropy change $-\Delta S_M$ from the magnetization data was estimated using a Maxwell relation.

B. Scaling analysis

According to the scaling hypothesis, the second-order phase transition around the Curie point T_c is characterized by a set of interrelated critical exponents $\alpha, \beta, \gamma, \delta, \eta, \nu$ and a magnetic equation of state [26]. The exponent α can be obtained from specific heat and β and γ from spontaneous magnetization M_s and inverse initial susceptibility χ_0^{-1} , below and above T_c , respectively, while δ is the critical isotherm exponent. The mathematical definitions of the exponents from magnetization measurement are given below:

$$M_s(T) = M_0(-\varepsilon)^\beta, \quad \varepsilon < 0, T < T_c, \quad (1)$$

$$\chi_0^{-1}(T) = (h_0/m_0)\varepsilon^\gamma, \quad \varepsilon > 0, T > T_c, \quad (2)$$

$$M = DH^{1/\delta}, \quad T = T_c, \quad (3)$$

where $\varepsilon = (T - T_c)/T_c$ is the reduced temperature, and $M_0, h_0/m_0$, and D are the critical amplitudes [27].

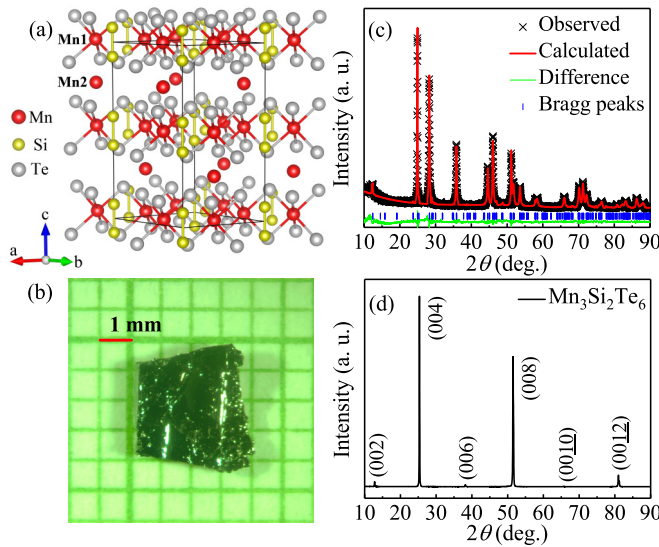


FIG. 1. (a) Crystal structure and (b) representative single crystal of $\text{Mn}_3\text{Si}_2\text{Te}_6$. (c) Powder x-ray diffraction (XRD) and (d) single-crystal XRD patterns of $\text{Mn}_3\text{Si}_2\text{Te}_6$ at room temperature. The vertical tick marks represent Bragg reflections of the $P\bar{3}1c$ space group.

The magnetic equation of state in the critical region is expressed as

$$M(H, \varepsilon) = \varepsilon^\beta f_\pm(H/\varepsilon^{\beta+\gamma}), \quad (4)$$

where f_+ for $T > T_c$ and f_- for $T < T_c$, respectively, are the regular functions. Equation (4) can be further written in terms of scaled magnetization $m \equiv \varepsilon^{-\beta} M(H, \varepsilon)$ and scaled field $h \equiv \varepsilon^{-(\beta+\gamma)} H$ as

$$m = f_\pm(h). \quad (5)$$

This suggests that for true scaling relations and the right choice of β , γ , and δ values, scaled m and h will fall on universal curves above T_c and below T_c , respectively.

III. RESULTS AND DISCUSSIONS

The powder XRD pattern of $\text{Mn}_3\text{Si}_2\text{Te}_6$ confirms high purity of the single crystals, in which the observed peaks can be well fitted with the $P\bar{3}1c$ space group [Fig. 1(c)]. The determined lattice parameters $a = 7.046(2) \text{ \AA}$ and $c = 14.278(2) \text{ \AA}$ are very close to the reported values [24,25]. In the single-crystal XRD [Fig. 1(d)], only (00 l) peaks are detected, indicating that the crystal surface is parallel to the ab plane and perpendicular to the c axis.

Figure 2 presents the temperature dependence of magnetization measured in $H = 1$ and 50 kOe applied in the ab plane and parallel to the c axis, respectively. The magnetization is nearly isotropic in 50 kOe, however, significant magnetic anisotropy is observed in 1 kOe at low temperatures. The ordered moments lie primarily within the ab plane. An additional upturn well above T_c up to 300 K is clearly seen in the zero-field-cooling (ZFC) curve for $\mathbf{H} // \mathbf{ab}$, which may be associated with short-range order or the presence of correlated excitations in the paramagnetic region [25]. Isothermal magnetization at $T = 5$ K (insets in Fig. 2) shows saturation moment of $M_s \approx 1.6 \mu_B/\text{Mn}$ for $\mathbf{H} // \mathbf{ab}$ and a small FM component for

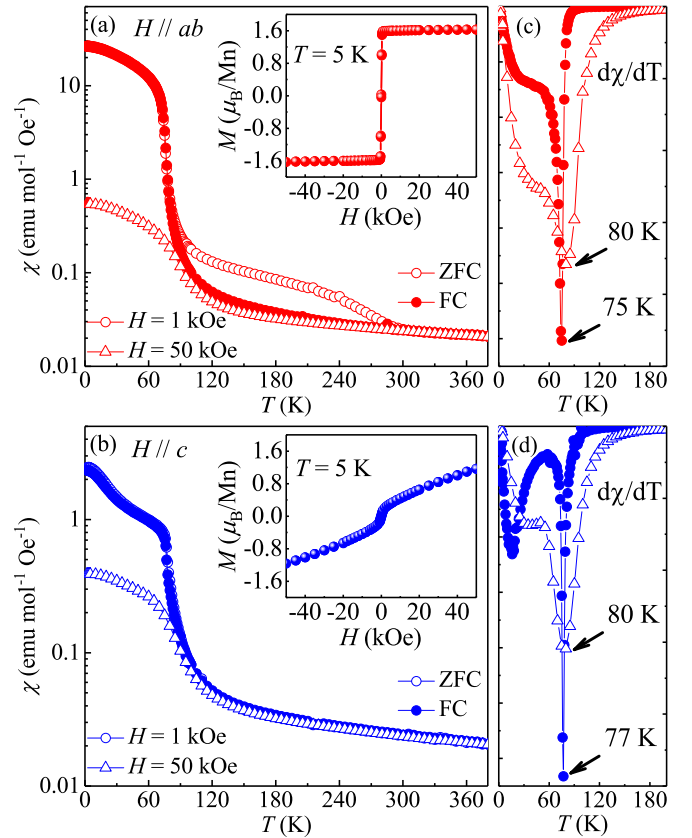


FIG. 2. Temperature dependence of dc magnetic susceptibility χ and corresponding $d\chi/dT$ for $\text{Mn}_3\text{Si}_2\text{Te}_6$ measured in the magnetic field $H = 1$ and 50 kOe applied (a),(c) in the ab plane and (b),(d) along the c axis, respectively. Insets: field dependence of magnetization measured at $T = 5$ K.

$\mathbf{H} // \mathbf{c}$. No remanent moment for either orientation confirms the crystal of high quality. The T_c can be roughly determined by the minimum of $d\chi/dT$ [Figs. 2(c) and 2(d)], i.e., $T_c = 75$ K for in-plane field and $T_c = 77$ K for out-of-plane field of 1 kOe, which shifts to $T_c = 80$ K in an increase field of 50 kOe [25].

From the Landau theory of phase transition, the Gibbs free energy G for FM-paramagnetic (PM) transition can be expressed as

$$G(T, M) = G_0 + aM^2 + bM^4 - MH, \quad (6)$$

where the equilibrium magnetization M is the order parameter, and the coefficients a and b are the temperature-dependent parameters. At equilibrium $\partial G/\partial M = 0$ (i.e., energy minimization) and the magnetic equation of state can be expressed as

$$H/M = 2a + 4bM^2. \quad (7)$$

Thus, the Arrott plot of M^2 vs H/M should appear as parallel straight lines for different temperatures above and below T_c in the high field region [28]. The intercepts of M^2 on the H/M axis is negative or positive depending on phenomena below or above T_c and the line at T_c passes through the origin. In order to properly determine the T_c as well as the critical exponents β , γ , and δ , the modified Arrott plot with a self-consistent method was used [29,30]. Figure 3 presents

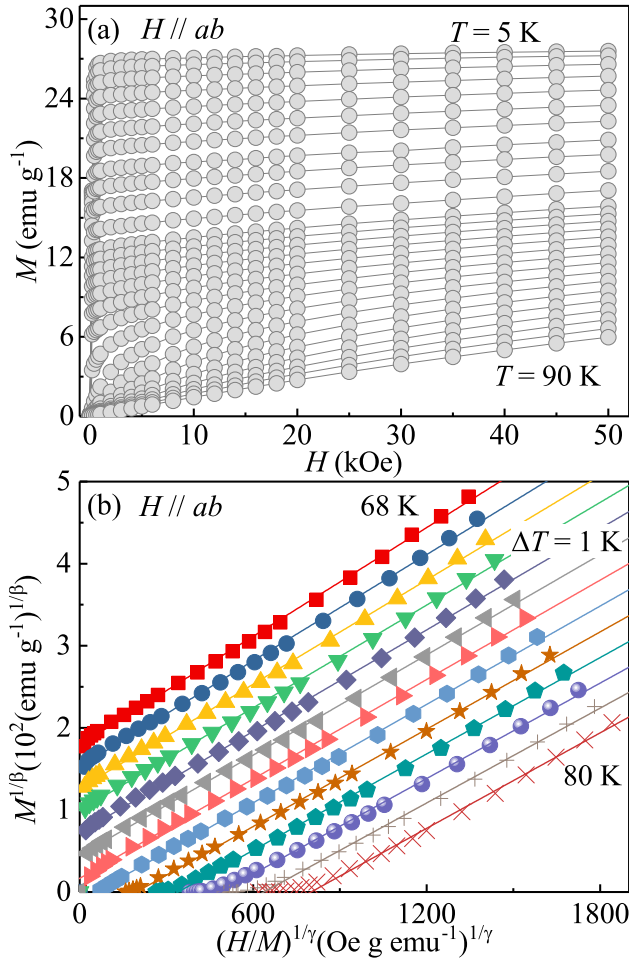


FIG. 3. (a) Typical initial isothermal magnetization curves measured in \mathbf{H}/\mathbf{ab} from 5 to 90 K for $\text{Mn}_3\text{Si}_2\text{Te}_6$. (b) the modified Arrott Plot around T_c for the optimum fitting with $\beta = 0.41$ and $\gamma = 1.21$.

the initial isotherms ranging from 5 to 90 K and the modified Arrott plot of $M^{1/\beta}$ vs $(H/M)^{1/\gamma}$ around T_c for $\text{Mn}_3\text{Si}_2\text{Te}_6$. This gives $\chi_0^{-1}(T)$ and $M_s(T)$ as the intercepts on the H/M axis and positive M^2 axis, respectively.

Figure 4(a) exhibits the final $M_s(T)$ and $\chi_0^{-1}(T)$ as a function of temperature. According to Eqs. (1) and (2), the critical exponents $\beta = 0.41(1)$ with $T_c = 74.21(1)$ K, and $\gamma = 1.25(1)$ with $T_c = 74.25(3)$ K, are obtained. In addition, there is also the Kouvel-Fisher (KF) relation [31],

$$M_s(T)[dM_s(T)/dT]^{-1} = (T - T_c)/\beta, \quad (8)$$

$$\chi_0^{-1}(T)[d\chi_0^{-1}(T)/dT]^{-1} = (T - T_c)/\gamma. \quad (9)$$

Linear fittings to the plots of $M_s(T)[dM_s(T)/dT]^{-1}$ and $\chi_0^{-1}(T)[d\chi_0^{-1}(T)/dT]^{-1}$ vs T in Fig. 4(b) yield $\beta = 0.41(1)$ with $T_c = 74.18(8)$ K, and $\gamma = 1.21(2)$ with $T_c = 74.35(5)$ K. The third exponent δ can be calculated from the Widom scaling relation $\delta = 1 + \gamma/\beta$. From β and γ obtained with the modified Arrott plot and the Kouvel-Fisher plot, $\delta = 4.05(5)$ and $3.95(2)$ are obtained, respectively, which are close to the direct fits of δ taking into account that $M = DH^{1/\delta}$ near T_c [$\delta = 4.29(5)$ at 74 K and $3.40(2)$ at 75 K, inset in Fig. 4(a)].

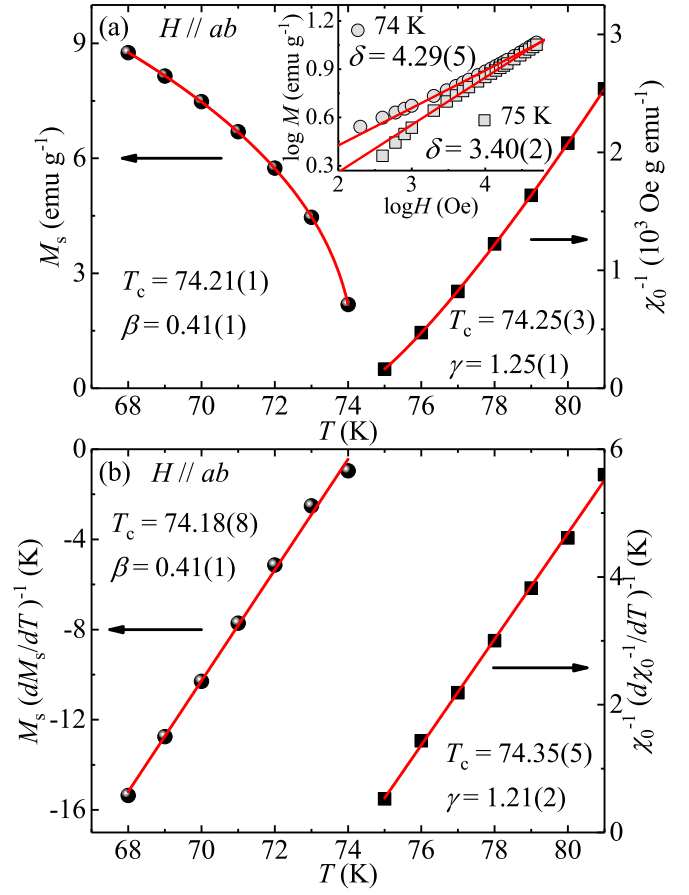


FIG. 4. (a) Temperature dependence of the spontaneous magnetization M_s (left) and the inverse initial susceptibility χ_0^{-1} (right) with solid fitting curves. Inset shows $\log M$ vs $\log H$ collected at 74 and 75 K with linear fitting curves. (b) Kouvel-Fisher plots of $M_s(dM_s/dT)^{-1}$ (left) and $\chi_0^{-1}(d\chi_0^{-1}/dT)^{-1}$ (right) with solid fitting curves.

Scaling analysis can be used to estimate the reliability of the obtained critical exponents and T_c . From Eq. (5), scaled m vs scaled h , all the data collapse on two separate branches below and above T_c , as depicted in Fig. 5. The scaling equation of state takes another form,

$$\frac{H}{M^\delta} = k\left(\frac{\varepsilon}{H^{1/\beta}}\right), \quad (10)$$

where $k(x)$ is the scaling function. From Eq. (10), all the data should also fall into a single curve. This is indeed seen (inset in Fig. 5); the $MH^{-1/\delta}$ vs $\varepsilon H^{-1/(\beta\delta)}$ experimental data for $\text{Mn}_3\text{Si}_2\text{Te}_6$ collapse into a single curve and the T_c locates at the zero point of the horizontal axis. The well-rescaled curves further confirm the reliability of the obtained critical exponents.

Next, it is important to understand the nature as well as the range of interaction in this material. In a homogeneous magnet the universality class of the magnetic phase transition depends on the exchange distance $J(r)$. In renormalization group theory analysis the interaction decays with distance r as

$$J(r) \approx r^{-(3+\sigma)}, \quad (11)$$

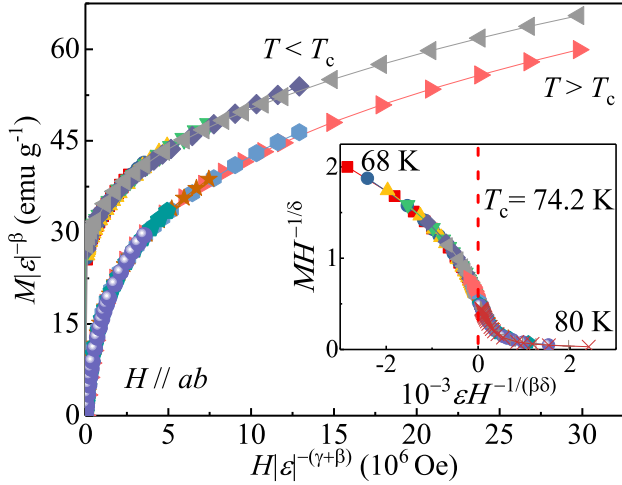


FIG. 5. Scaled magnetization m vs scaled field h below and above T_c for $\text{Mn}_3\text{Si}_2\text{Te}_6$. Inset: the rescaling of the $M(H)$ curves by $MH^{-1/\delta}$ vs $\varepsilon H^{-1/(\beta\delta)}$.

where σ is a positive constant [32]. Moreover, the susceptibility exponent γ is predicted as

$$\gamma = 1 + \frac{4}{d} \left(\frac{n+2}{n+8} \right) \Delta\sigma + \frac{8(n+2)(n-4)}{d^2(n+8)^2} \times \left[1 + \frac{2G(\frac{d}{2})(7n+20)}{(n-4)(n+8)} \right] \Delta\sigma^2, \quad (12)$$

where $\Delta\sigma = (\sigma - \frac{d}{2})$ and $G(\frac{d}{2}) = 3 - \frac{1}{4}(\frac{d}{2})^2$, n is the spin dimensionality [33]. When $\sigma > 2$, the Heisenberg model is valid for 3D isotropic magnet, where $J(r)$ decreases faster than r^{-5} . When $\sigma \leq 3/2$, the mean-field model is satisfied, expecting that $J(r)$ decreases slower than $r^{-4.5}$. In the present case, $\sigma = 1.79$, then the correlation length critical exponent $\nu = 0.676$ ($\nu = \gamma/\sigma$), and $\alpha = -0.028$ ($\alpha = 2 - \nu d$). It is found that the magnetic exchange distance decays as $J(r) \approx r^{-4.79}$, which lies between that of the 3D Heisenberg model and mean-field model.

Then we estimate its magnetic entropy change

$$\Delta S_M(T, H) = \int_0^H \left[\frac{\partial S(T, H)}{\partial H} \right]_T dH. \quad (13)$$

With the Maxwell's relation $[\frac{\partial S(T, H)}{\partial H}]_T = [\frac{\partial M(T, H)}{\partial T}]_H$, it can be further written as [34]:

$$\Delta S_M(T, H) = \int_0^H \left[\frac{\partial M(T, H)}{\partial T} \right]_H dH. \quad (14)$$

In the case of magnetization measured at small discrete magnetic field and temperature intervals [Fig. 3(a)], $\Delta S_M(T, H)$ could be practically approximated as,

$$\Delta S_M(T_i, H) = \frac{\int_0^H M(T_i, H) dH - \int_0^H M(T_{i+1}, H) dH}{T_i - T_{i+1}}. \quad (15)$$

Figure 6(a) gives the calculated $-\Delta S_M$ as a function of temperature. All the $-\Delta S_M(T, H)$ curves present a pronounced peak at T_c , and the peak broadens asymmetrically on both sides with increasing field. The maximum value of $-\Delta S_M$ reaches

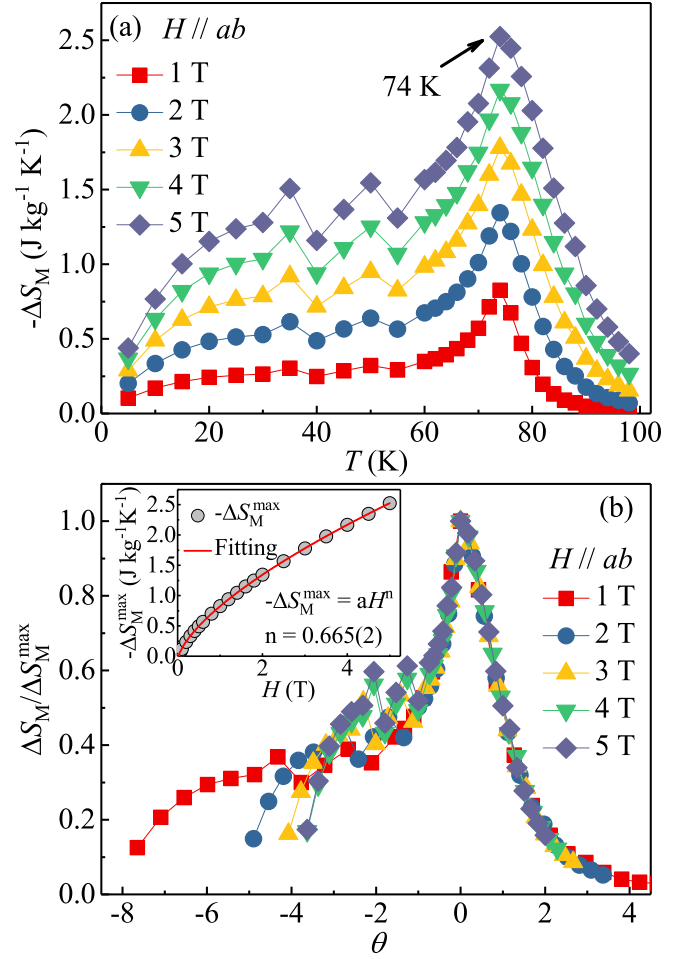


FIG. 6. (a) The magnetic entropy change $-\Delta S_M$ obtained from magnetization at various magnetic fields change in the ab plane. (b) Normalized ΔS_M as a function of the rescaled temperature θ . Inset: magnetic field dependence of the maximum magnetic entropy change $-\Delta S_M^{\max}$ with power law fitting in red solid line.

$2.53 \text{ J kg}^{-1} \text{ K}^{-1}$ with in-plane field change of 5 T. This is comparable to $\text{Mn}_{2-x}\text{Cr}_x\text{Sb}$ but smaller than in $\text{MnFeP}_{0.45}\text{As}_{0.55}$ or $\text{Gd}_5\text{Ge}_2\text{Si}_2$ magnetic refrigerant materials [35,36].

Scaling analysis of $-\Delta S_M$ can be built by normalizing all the $-\Delta S_M$ curves against the respective maximum $-\Delta S_M^{\max}$, namely, $\Delta S_M/\Delta S_M^{\max}$ by rescaling the temperature θ as defined in the following equations [37],

$$\theta_- = (T_{\text{peak}} - T)/(T_{r1} - T_{\text{peak}}), \quad T < T_{\text{peak}}, \quad (16)$$

$$\theta_+ = (T - T_{\text{peak}})/(T_{r2} - T_{\text{peak}}), \quad T > T_{\text{peak}}, \quad (17)$$

where T_{r1} and T_{r2} are the temperatures of the two reference points that have been selected as those corresponding to $\Delta S_M(T_{r1}, T_{r2}) = \frac{1}{2} \Delta S_M^{\max}$. Following this method, all the $-\Delta S_M(T, H)$ curves in various fields collapse into a single curve in the vicinity of T_c [Fig. 6(b)]. In the framework of the mean-field theory, $-\Delta S_M^{\max} = -1.07qR(g\mu_B JH/k_B T_c)^{2/3} \propto H^{2/3}$, where q is the number of magnetic ions, R is the gas constant, and g is the Lande factor [38]. In fact, more universally, it should follow a power law relation, $-\Delta S_M^{\max} = aH^n$, where n depends on the magnetic

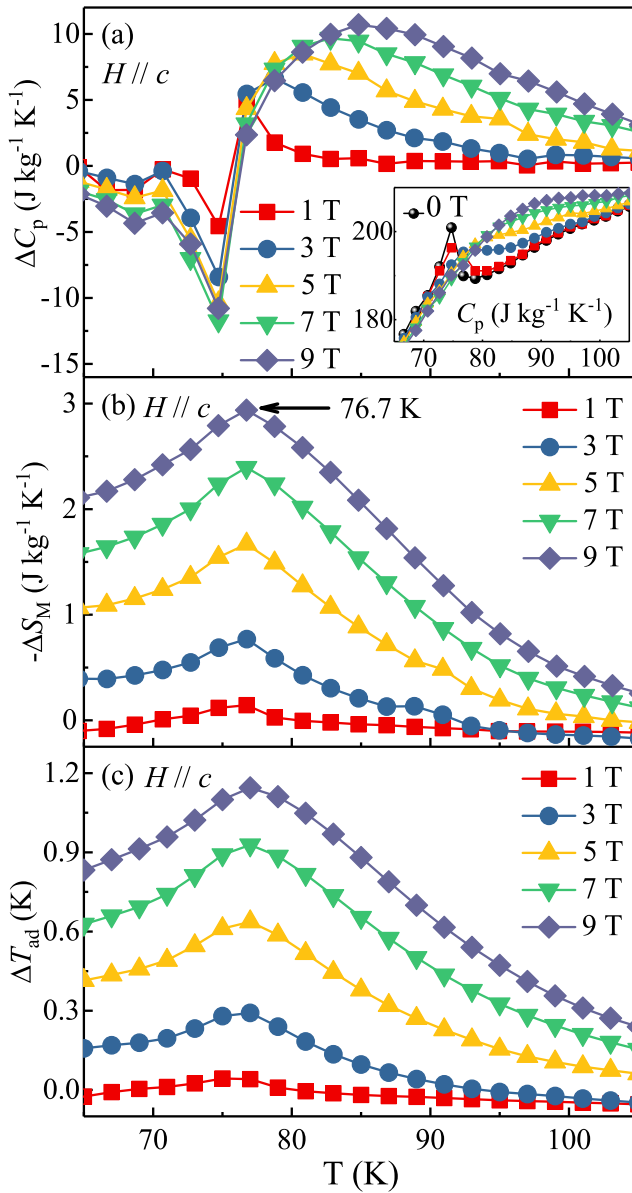


FIG. 7. Temperature dependences of (a) the specific heat change ΔC_p , (b) the magnetic entropy change $-\Delta S_M$, and (c) the adiabatic temperature change ΔT_{ad} for $\text{Mn}_3\text{Si}_2\text{Te}_6$ at the indicated fields. Inset shows the temperature dependence of specific heat C_p .

state of the sample. Fitting of the field dependence of $-\Delta S_M^{\max}$ with $\mathbf{H} // \mathbf{ab}$ gives $n = 0.665(2)$ [inset in Fig. 6(b)], close to the typical value of $2/3$ within the mean-field model.

Finally, we also estimate the $-\Delta S_M$ from heat capacity measurement with out-of-plane fields up to 9 T. The λ peak observed at $T_c = 74.7$ K in zero field [inset in Fig. 7(a)], corresponding well to the PM-FM transition, is gradually suppressed in fields. Figure 7(a) shows the calculated heat capacity change $\Delta C_p = C_p(T, H) - C_p(T, 0)$ as a function of temperature in various fields. Obviously, $\Delta C_p < 0$ for $T < T_c$ and $\Delta C_p > 0$ for $T > T_c$, while it changes sharply from negative to positive at T_c , corresponding to the change from FM to PM. The entropy $S(T, H)$ can be deduced by

$$S(T, H) = \int_0^T \frac{C_p(T, H)}{T} dT. \quad (18)$$

Assuming the electronic and lattice contributions are not field dependent and in an adiabatic process of changing the field, the magnetic entropy change $-\Delta S_M$ can be straightly obtained $-\Delta S_M(T, H) = S_M(T, H) - S_M(T, 0)$. The adiabatic temperature change ΔT_{ad} caused by the field change can be obtained by $\Delta T_{ad}(T, H) = T(S, H) - T(S, 0)$, where $T(S, H)$ and $T(S, 0)$ are the temperatures in the field $H \neq 0$ and $H = 0$, respectively, at constant total entropy $S(T, H)$. Figures 7(b) and 7(c) exhibit the temperature dependence of $-\Delta S_M$ and ΔT_{ad} estimated from heat capacity with out-of-plane field. The maxima of $-\Delta S_M$ and ΔT_{ad} increase with increase field and reach the values of $2.94 \text{ J kg}^{-1} \text{ K}^{-1}$ and 1.14 K, respectively, with the field change of 9 T.

IV. CONCLUSIONS

In summary, we have studied the critical behavior and magnetocaloric effect around the FM-PM transition in $\text{Mn}_3\text{Si}_2\text{Te}_6$ single crystal. The ferrimagnetic transition in $\text{Mn}_3\text{Si}_2\text{Te}_6$ is identified to be second order in nature. The critical exponents β , γ , and δ estimated from various techniques match reasonably well and follow the scaling equation, suggesting a long-range magnetic interaction with the exchange distance decaying as $J(r) \approx r^{-4.79}$. Magnetocaloric effect is about one order of magnitude smaller when compared to other magnetorefrigerant candidate materials.

ACKNOWLEDGMENTS

This work was supported by the US Department of Energy, Office of Basic Energy Sciences as part of the Computational Material Science Program.

- [1] M. A. McGuire, G. Clark, S. KC, W. M. Chance, G. E. Jellison, Jr., V. R. Cooper, X. D. Xu, and B. C. Sales, *Phys. Rev. Materials* **1**, 014001 (2017).
- [2] M. A. McGuire, H. Dixit, V. R. Cooper, and B. C. Sales, *Chem. Mater.* **27**, 612 (2015).
- [3] B. Huang, G. Clark, E. Navarro-Moratalla, D. R. Klein, R. Cheng, K. L. Seyler, D. Zhong, E. Schmidgall, M. A. McGuire,

- D. H. Cobden, W. Yao, D. Xiao, P. Jarillo-Herrero, and X. D. Xu, *Nature (London)* **546**, 270 (2017).
- [4] C. Gong, L. Li, Z. L. Li, H. W. Ji, A. Stern, Y. Xia, T. Cao, W. Bao, C. Z. Wang, Y. Wang, Z. Q. Qiu, R. J. Cava, S. G. Louie, J. Xia, and X. Zhang, *Nature (London)* **546**, 265 (2017).
- [5] K. L. Seyler, D. Zhong, D. R. Klein, S. Guo, X. Zhang, B. Huang, E. Navarro-Moratalla, L. Yang, D. H. Cobden, M. A. McGuire,

- W. Yao, D. Xiao, P. Jarillo-Herrero, and X. D. Xu, *Nat. Phys.* **14**, 277 (2018).
- [6] S. Jiang, L. Li, Z. Wang, K. F. Mak, and J. Shan, *Nat. Nanotech.* **13**, 549 (2018).
- [7] B. Huang, G. Clark, D. R. Klein, D. MacNeill, E. Navarro-Moratalla, K. L. Seyler, N. Wilson, M. A. McGuire, D. H. Cobden, D. Xiao, W. Yao, P. Jarillo-Herrero, and X. D. Xu, *Nat. Nanotech.* **13**, 544 (2018).
- [8] G. Ouvrard, E. Sandre, and R. Brec, *J. Solid State Chem.* **73**, 27 (1988).
- [9] V. Carteaux, G. Ouvrard, J. C. Grenier, and Y. Lalignant, *J. Magn. Mater.* **94**, 127 (1991).
- [10] V. Carteaux, D. Brunet, G. Ouvrard, and G. André, *J. Phys.: Condens. Matter* **7**, 69 (1995).
- [11] L. D. Casto, A. J. Clune, M. O. Yokosuk, J. L. Musfeldt, T. J. Williams, H. L. Zhuang, M. W. Lin, K. Xiao, R. G. Hennig, B. C. Sales, J. Q. Yan, and D. Mandrus, *APL Mater.* **3**, 041515 (2015).
- [12] X. Zhang, Y. L. Zhao, Q. Song, S. Jia, J. Shi, and W. Han, *Jpn. J. Appl. Phys.* **55**, 033001 (2016).
- [13] H. L. Zhuang, Y. Xie, P. R. C. Kent, and P. Ganesh, *Phys. Rev. B* **92**, 035407 (2015).
- [14] M. W. Lin, H. L. Zhuang, J. Q. Yan, T. Z. Ward, A. A. Purotzky, C. M. Rouleau, Z. Gai, L. B. Liang, V. Meunier, B. G. Sumpter, P. Ganesh, P. R. C. Kent, D. B. Geohegan, D. G. Mandrus, and K. Xiao, *J. Mater. Chem. C* **4**, 315 (2016).
- [15] X. X. Li, and J. L. Yang, *J. Mater. Chem. C* **2**, 7071 (2014).
- [16] X. F. Chen, J. S. Qi, and D. N. Shi, *Phys. Lett. A* **379**, 60 (2015).
- [17] N. Sivadas, M. W. Daniels, R. H. Swendsen, S. Okamoto, and D. Xiao, *Phys. Rev. B* **91**, 235425 (2015).
- [18] J. P. Liu, S. Y. Park, K. F. Garrity, and D. Vanderbilt, *Phys. Rev. Lett.* **117**, 257201 (2016).
- [19] B. J. Liu, Y. M. Zou, L. Zhang, S. M. Zhou, Z. Wang, W. K. Wang, Z. Qu, and Y. H. Zhang, *Sci. Rep.* **6**, 33873 (2016).
- [20] G. T. Lin, H. L. Zhuang, X. Luo, B. J. Liu, F. C. Chen, J. Yan, Y. Sun, J. Zhou, W. J. Lu, P. Tong, Z. G. Sheng, Z. Qu, W. H. Song, X. B. Zhu, and Y. P. Sun, *Phys. Rev. B* **95**, 245212 (2017).
- [21] Y. Liu and C. Petrovic, *Phys. Rev. B* **96**, 054406 (2017).
- [22] T. F. Guo, Z. W. Ma, G. T. Lin, X. Luo, Y. B. Hou, Y. P. Sun, Z. G. Sheng, and Q. Y. Lu, [arXiv:1803.06113](https://arxiv.org/abs/1803.06113).
- [23] R. Rimet, C. Schlenker, and H. Vincent, *J. Magn. Magn. Mater.* **25**, 7 (1981).
- [24] H. Vincent, D. Leroux, D. Bijaoui, R. Rimet, and C. Schlenker, *J. Solid State Chem.* **63**, 349 (1986).
- [25] A. F. May, Y. Liu, S. Calder, D. S. Parker, T. Pandey, E. Cakmak, H. Cao, J. Yan, and M. A. McGuire, *Phys. Rev. B* **95**, 174440 (2017).
- [26] H. E. Stanley, *Introduction to Phase Transitions and Critical Phenomena* (Oxford University Press, London, New York, 1971).
- [27] M. E. Fisher, *Rep. Prog. Phys.* **30**, 615 (1967).
- [28] A. Arrott, *Phys. Rev.* **108**, 1394 (1957).
- [29] W. Kellner, M. Fähnle, H. Kronmüller, and S. N. Kaul, *Phys. Status Solidi B* **144**, 387 (1987).
- [30] A. K. Pramanik and A. Banerjee, *Phys. Rev. B* **79**, 214426 (2009).
- [31] J. S. Kouvel and M. E. Fisher, *Phys. Rev.* **136**, A1626 (1964).
- [32] M. E. Fisher, S. K. Ma, and B. G. Nickel, *Phys. Rev. Lett.* **29**, 917 (1972).
- [33] S. F. Fischer, S. N. Kaul, and H. Kronmüller, *Phys. Rev. B* **65**, 064443 (2002).
- [34] J. Amaral, M. Reis, V. Amaral, T. Mendonc, J. Araujo, M. Sa, P. Tavares, and J. Vieira, *J. Magn. Magn. Mater.* **290**, 686 (2005).
- [35] L. Caron, F. Miao, J. C. P. Klaasse, S. Gama, and E. Brück, *Appl. Phys. Lett.* **103**, 112404 (2013).
- [36] O. Tegus, E. Brück, K. H. J. Buschow, and F. R. de Boer, *Nature (London)* **415**, 150 (2002).
- [37] V. Franco and A. Conde, *Int. J. Refrig.* **33**, 465 (2010).
- [38] H. Oesterreicher and F. T. Parker, *J. Appl. Phys.* **55**, 4334 (1984).

Correction: Missing support information in the Acknowledgment section has been inserted.

Second Correction: Some statements in the Acknowledgment section have been updated.